Redox, Magnetic and Structural Properties of α-$NaMnO_2$ Cathode Material Analysed by Fitting-free DFT+U Calculations, Parameterised by Linear Response Approach

Maxim Shishkin[*,†] and Hirofumi Sato[†,‡,¶]

†*Elements Strategy Initiative for Catalysts and Batteries (ESICB), Kyoto University, Nishikyo-ku, Kyoto 615-8520, Japan*

‡*Department of Molecular Engineering, Kyoto University, Nishikyo-ku, Kyoto 615-8510, Japan*

¶*Fukui Institute for Fundamental Chemistry, Kyoto University, Japan*

E-mail: shishkin.maxim.6c@kyoto-u.ac.jp

Abstract

Evaluation of electrochemical properties of cathode materials is desirable to be performed without recourse to empirical fitting as well as to be able to reproduce experimental measurements with a high level of accuracy. In this work we present the results of our calculations of voltage profile of α-$NaMnO_2$ cathode material, using DFT+U method, parameterized computationally by the linear response approach. Our calculations reveal an improved agreement with experimental voltage curve as compared to DFT+U calculations with a fitted and fixed U parameter, particularly for high voltages. Additionally, we also analyse how magnetic ordering of $NaMnO_2$ changes upon the process of deintercalation when Na charge carriers are removed, leading to the change of

oxidation state of Mn cations of the bulk. We demonstrate that antiferromagnetic ordering, observed experimentally for $NaMnO_2$ and $LiMnO_2$ indeed corresponds to lower energy with changing to ferromagnetic ordering upon removal of 40-50% of Na ions or more. Analysis of previously identified configurations Na_xMnO_2 (using experimental and theoretical methods) has also shown the importance of numerical evaluation of U parameter for better agreement with experimental findings.

1. Introduction

Successful development of electrochemical energy storage devices, such as rechargable batteries is one of the prerequisites for future economic growth and further sustainment of standards of life. The key electrochemical property of a battery is dependence of operating voltage from concentration of charge carrier cations, such as Li. Larger operating potentials and larger amounts of charge carriers, that can be removed and re-inserted into electrode materials (defined as an electrode capacity), could result in a higher operating energy density, allowing for a wider range of possible applications of battery storage systems. Another important aspect of development of battery technology is the need for low cost materials, that can be used as constituent battery parts. For instance, a widely used $LiCoO_2$ cathode material, contains relatively expensive Co element.[1] Moreover, a widespread application of Li-ion batteries exposed the lack of Li used as a charge carrier in Li-ion batteries, pushing towards substitution of Li by other, more abundant and geographically dispersed elements such as Na.[2]

In this regard $NaMnO_2$ layered oxide offers a potentially attractive option as a cathode material which contains only inexpensive elements such as Na and Mn and also possesses high energy density.[3–5] The structural properties of $NaMnO_2$ have been studied in detail in 1980s by Delmas and coworkers, who analysed various structural arrangements of such materials, known as polymorphs.[6] Delmas et al provided a classification of observed polymorphs, based on the type of a cage of nearest oxygen neighbours of Mn cations (octahedral, tetrahedral

or prismatic, denoted as O, T and P) and the type of oxygen stacking, indicated by the number of O-Mn-O trilayers in a crystal cell. For instance, O3 notation could be used for indicating the presence of three trilayers in the crystal cell, in contrast to O1 structures, where a crystal cell contains only one O-Mn-O trilayer. Subsequently voltage profiles of O3-$NaMnO_2$ polymorph (also denoted as α-$NaMnO_2$ in some works) have been also measured.[7] The measurements revealed that deintercalation voltage profile, which corresponds to Na removal from $NaMnO_2$ is characterized by a close to a constant plateau upon removal of less than a half of Na cations from initial stoichiometric $NaMnO_2$.[7] Further removal of Na leads to voltage increase at lower Na concentrations.[7] The measurements of voltage profile also demonstrated the presence of hysteresis within the intercalation/de-intercalation cycle, manifested by slightly lower voltages upon reinsertion of Na (intercaltion) as compared to voltages, which correspond to Na removal (deintercalation) for the same Na concentrations.[7]

The voltage profile of $NaMnO_2$ (assuming O3 structure) has been also evaluated using *ab initio* modeling. Toumar et al performed DFT+U calculation of voltage profiles for a large set of layered oxides, that can be potentially used as cathodes of Na-ion batteries, including $NaMnO_2$.[8] Calculations of Toumar et al have shown a good agreement with a measured profile, predicting a nearly constant voltage at the initial stage of Na removal (up to about 50%) with subsequent voltage increase as more Na are extracted.[8] However, at low Na concentrations calculations of Toumar et al predicted substantially underestimated voltage as compared to experiment. More recently, Zhang et al also performed DFT+U evaluation of a voltage profile of Na_xMnO_2.[9] In contrast to a gradual voltage increase upon removal of about a half of Na, their work predicted a two-plateaux character with a large and single step at 75% of Na concentration.[9]

In general case, accurate calculation of redox voltages of cathode materials is a challenging task, owing to poor ability of local DFT functionals to adequately describe interactions between strongly localised d-orbitals of transition metal cations of cathode materials.[10] DFT+U approach is a common choice for treatment of strong correlation of localized states

of transition metals, allowing for reasonably accurate and also robust calculations of large computational cells (100 atoms or more).[11–14] However, one of the shortcomings of DFT+U method is a common reliance on empirical determination of U parameters, required for parameterisation of computational framework.[15] Alternatively, redox voltages could be calculated employing very accurate *ab initio* methods, such as quantum Monte Carlo as has been done recently for $LiNiO_2$ cathode material.[16] It should be noted that routine application of quantum Monte Carlo technique, particularly for evaluation of voltage profiles, that require calculations of a very large number of models, could not be feasible, at least in a near future. Therefore development and testing of other methods, that would allow accurate and computationally tractable calculations is still of a great interest.

Evaluation of U parameter computationally, particularly using the linear response method is an alternative approach,[17–22] which permits determination of U fully avoiding fitting to experimental data. Previous works,[23] including several, performed by us,[20,24] have shown that average redox voltages can be calculated with a reasonable accuracy for various cathode materials, adopting the values of U parameters determined using linear response parameterisation. This strategy seems also very appropriate for future studies where several types of transition metal cations are introduced into a cathode material, requiring adjustment of U values obtained via fitting procedure for the case of more simple structures with one type of TM cations.[25]

Although average redox voltages have been calculated previously using computationally defined U parameters within DFT+U framework, this approach, to the best of our knowledge, has not been tested for evaluation of an entire voltage profile of a cathode material, which is a more challenging task. Indeed, in case of evaluation of a voltage profile, the search for the low energy structures at various concentrations of Li or Na cations has to be performed. Moreover, the accuracy of a computation framework in such a study is subject to a more rigorous test, requiring accurate evaluation of energy differences for structures with various Li or Na concentrations rather than a single difference between the energies of

fully intercalated and deintercalated structures as is done for evaluation of an average redox potential.

In this work we perform testing of accuracy of DFT+U method, parameterised by linear response approach, applying it to evaluation of a voltage profile of α-$NaMnO_2$ cathode material. Additionally, we also address two aspects, that have to be further elaborated in the study of desodiation of $NaMnO_2$. Firstly, we analyse which type of magnetic ordering may correspond to lower energies of the structures upon Na removal from $NaMnO_2$. To date, experimental literature clearly indicates that both $NaMnO_2$ and $LiMnO_2$ structures adopt antiferromagnetic (AFM) ordering at temperatures close to 0K.[26,27] This aspect seems to be neglected in previous studies of $NaMnO_2$, where ferromagnetic (FM) ordering is usually assumed for all Na concentrations.[8] As we shall discuss in the subsequent sections, from computational viewpoint AFM ordering often requires larger supercells for analysis of partially deintercalated structures at specific Na concentrations as compared to ferromagnetically ordered configurations. Moreover, computational settings for AFM ordering is more complicated and also error-prone particularly for a large number of studied configurations with different types of computational cells as compared to a more straightforward and simple FM case, further adding to complexity of this study.

Second important aspect is analysis of recently identified partially desodiated structures, which have been characterised experimentally and computationally.[28,29] In this work we discuss a relative stability of these identified structures with respect to low energy configurations we constructed via simple removal of Na cations from employed computational cells of $NaMnO_2$. We also compare how these low energy structures are featured in computed voltage profiles obtained via DFT+U calculations, parameterised by linear response method and DFT+U with a fixed value of U parameter as is usually done in the literature to date.

2. Methods

2.1 Energy calculation

For all *ab initio* calculations we have employed the VASP package.[30] PBE functional has been used for treatment of exchange correlation effects[31] with additional Hubbard correction terms for *d*-states of Mn, taken in the form, proposed by Dudarev and coworkers.[32] For parameterisation of DFT+U calculations we have used the linear response (LR) approach.[20] We calculated U values (these are so-called effective U_{eff}, defined as U_{eff}=$U - J$; in this work we refer to them simply as U) for each Mn cation of a studied computational cell, including Mn^{3+} and Mn^{4+}. Subsequently an averaged U has been calculated as a sum of all computed U, divided by the number of Mn cations. Then this averaged U has been applied for all Mn, present in a studied cell and recalculated unto self-consistency as discussed in our previous work.[33] Self-consistency cycle was considered converged when the value of averaged U changes less than by 0.01eV as compared to the previous iteration.

The electronic states have been expanded into the plane waves with characteristic cut off energy of 600 eV. The PAW approach has been adopted for the treatment of interactions between valence electrons and the cores of all atoms, present in the studied structures.[34,35] We performed complete optimisation of atomic positions and full cell relaxation until atomic forces did not exceed 0.01eV/Å. The Monkhorst-Pack sampling of a Brilloiun zone[36] is a challenging issue in our study as the cells of various types and Na concentrations have been employed. We provide further details about the choices of k-point mech in the Supporting Material Section.

2.2 Computational cells

The structure of α-$NaMnO_2$ defined experimentally in the paper of Parant et al[37] is shown in Fig. 1. The aforementioned AFM ordering of stoichiometric $NaMnO_2$ and $LiMnO_2$[26,27] is also shown in Fig. 1. Although short-range two- and one-dimensional spin correlations

occur at higher temperatures for fully sodiated $NaMnO_2$,[38] these usually can not be assessed by standard DFT implementations, which allow evaluation of materials electronic structure only for absolute zero temperature.

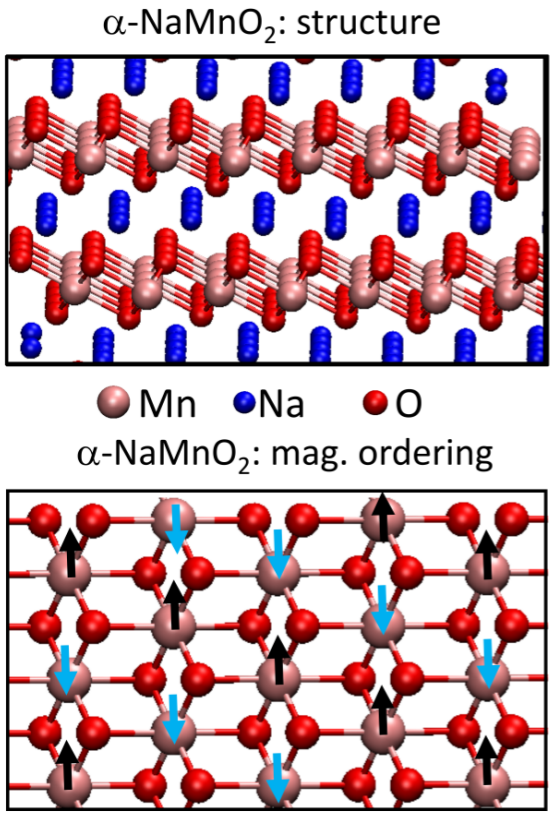

Figure 1: The optimised structure of α-$NaMnO_2$ (top). AFM ordering in the plane of O-Mn-O trilayer, according to the experimental measurements[26,27] is shown below.

Our recent DFT+U analysis of α- and β-$NaMnO_2$ polymorphs also revealed that in fully sodiated case both structures favor AFM ordering over FM arrangement in complete agreement with experimental observations.[33] However, favorable magnetic ordering might be different at lower Na concentrations as we show in subsequent sections. We should note that any structure with a specific Na concentration and positions of Na cations possesses a complex unique magnetic ordering that corresponds to the most stable ground state. A search for such ordering can be performed computationally as has been done recently for Mn_2O_3.[39] However, given a vast configurational space of possible orientations of magnetic moments on transition metal cations even for a single configuration of desodiated structure,

this method is not practical for our case where a large number of desodiated structures have been computed (747 configurations). For this reason, we adopted a simpler approach where we impose only two types of magnetic orderings on all studied configurations: AFM ordering mentioned above and commonly used FM ordering.

The voltage profile was determined using standard expression:[40]

$$V(x_1 < x < x_2) = -\frac{E(x_2) - E(x_1)}{e(x_2 - x_1)} + \frac{E(Na)}{e} \quad (1)$$

where $E(x_1)$ and $E(x_2)$ are total energies of supercells with x_1 and x_2 concentrations of Na and $E(Na)$ is the energy of Na cation in Na bulk, e is the charge of an electron. The values of $E(x_1)$ and $E(x_2)$ should correspond to the ground state structures, which possess the minimal total energies for respective concentrations x_1 and x_2.

We have employed the CASM software[41–44] in order to generate symmetrically non-equivalent structures with various concentrations of Na and also various positions of Na cations in partially desodiated $NaMnO_2$. The details of preparation of input geometry of partially desodiated cells are provided in the Supporting Material Section.

3. Results: evaluation of voltage profile

3.1 Calculation with fixed value of U=4.0eV

Our analysis of voltage profile starts from the search of ground state configurations of Na_xMnO_2 at various Na concentrations. Supporting Material Section provides the details of evaluation of the convex hull for FM and AFM ordering. Based on the results of calculations for two types of magnetic ordering, it is possible to determine which magnetic ordering is more favorable at each studied Na concentration. Using the ground states, present in the convex hull and comparing the total energies at the same Na concentration for FM and AFM cases, we have calculated the energy difference ΔE:

$$\Delta E(x) = E^{FM}(x) - E^{AFM}(x) \tag{2}$$

where $E^{FM}(x)$ and $E^{AFM}(x)$ are the total energies of the ground states with FM and AFM ordering at concentration x. The sign and the magnitude of ΔE allows to determine the type of a more favorable magnetic ordering at specific Na concentration. Fig. 2 provides dependence of ΔE from Na concentration, clearly demonstrating that at high concentrations AFM ordering is more favorable (above 62.5%), whereas at lower Na concentrations (<62.5%) FM ordering is certainly more preferential.

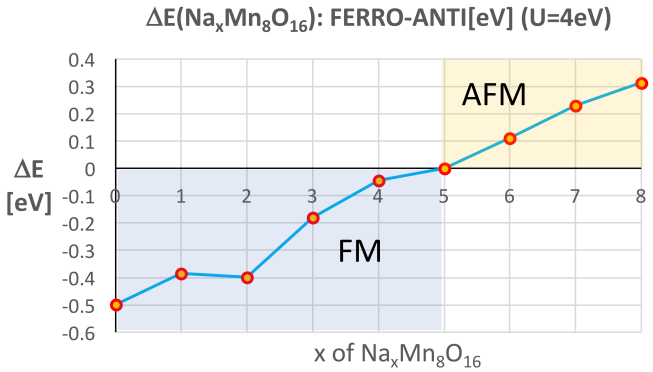

Figure 2: The energy difference between the ground state structures at FM and AFM ordering at various Na concentrations. AFM ordering prevails at high Na concentrations, whereas at low Na concentrations (<62.5%) FM is more favorable (highlighted by respective colours for convenience).

Using the calculated energetics and the findings on the preference of magnetic ordering at various Na concentrations, we have evaluated the voltage profile using eq. (1) as is shown in Fig. 3 (top). In addition to our evaluated voltage profile, we have provided the experimentally measured voltage of Ma et al.[7] For comparison with our calculations we have also presented the computed voltage profile for $NaMnO_2$ provided in the work of Toumar et al[8] in the middle graph of Fig. 3.

With regard to comparison with experimental measurements, we need to discuss three important aspects. First, which of the measured processes, intercalation or deintercalation should be used for comparison with computed results? Indeed, hysteresis of voltage, present

for instance in the studied $NaMnO_2$, is poorly understood to date although several interpretations have been provided recently.[45,46] Although it is beyond the scope of this study to address interpretation of hysteresis, for practical purposes we use a simple observation that compared to initial Na removal process, Na reinsertion should occur via less stable structures with higher energy. This conjecture is supported by the fact that reinsertion of Na occurs at lower voltages as compared to Na removal (the respective profile is below desodiation curve), which clearly indicates that respective configurations are higher in energy as compared to those that occur during Na removal at the same Na concentrations. Therefore, in our work we compared our calculated profile primarily with experimental deintercation curve, which corresponds to higher voltages and more stable configurations.

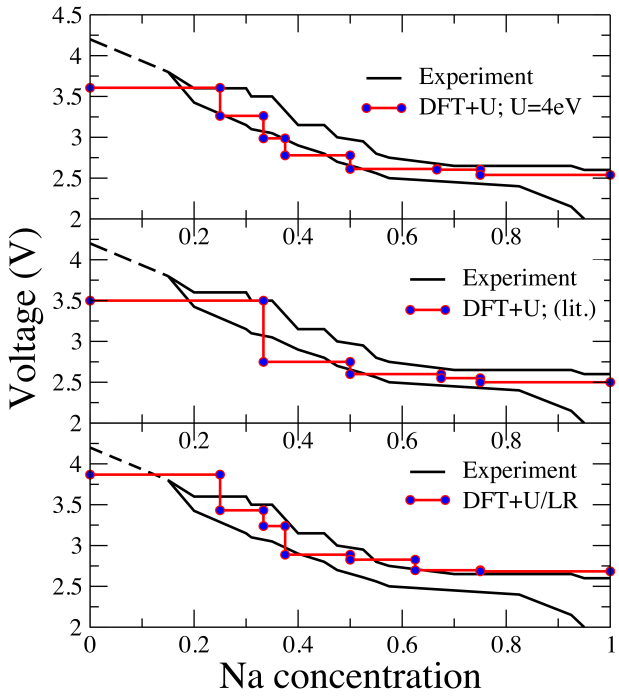

Figure 3: The computed voltage profiles of α-Na_xMnO_2: our computed results with the fixed value of U=4.eV (top); calculations, taken from the literature (Toumar et al,[8] middle); our calculations with U parameter, obtained via LR approach (bottom). The black solid line provides the results of measurements by Ma et al;[7] the broken line indicates the voltages, measured when the cell was charged up to high voltage of 4.2V.[7]

The second important question is which of the intercalation/deintercalation cycles, measured experimentally should be used for comparison with our results? This choice is necessary

due to the pronounced difference of measured voltage profiles for different measured cycles.[7] We believe that comparison with computational results should be performed for the first measured cycle as the structure of a studied material would then most closely correspond to the O3-$NaMnO_2$ configuration, studied herein. Indeed, a structure which is exposed to a removal of a large percentage of Na with subsequent reinsertion could have different structural properties (e.g. atomic defects and new phase formation) as compared to initially synthesized $NaMnO_2$. The experimentally observed drop of deintercalation voltages at high Na concentrations after the first cycle (by about 0.2V) is indicative of this.[7] A third aspect we need to mention is the necessity to compare our computed results with the measurements at very low Na concentrations. To do so, we included the results of measurements at high charging voltage (4.2 V) as indicated by the broken line in accordance with Fig. 5 of the paper of Ma et al.[7]

Now we proceed to comparison of results of our calculations with experimental measurements (particularly with deintercalation curve according to the argument presented above). We find that at low concentrations a slightly underestimated voltage plateau is predicted using our calculations. It should be noted that for subsequent measured cycles a lower value of voltage is observed in this range of Na concentrations resulting in a closer agreement with computed data.[7] However, as is discussed above, we tend to believe that comparison with the measurements of the first cycle is more appropriate here. At sodium concentrations below 50% or so, our calculations show a voltage increase in general agreement with experimental trend, although quantitatively computed voltages are lower than experimental. The underestimated computed voltages can be seen for some Na concentrations even when compared to intercalation curve in Fig. 3. At very low Na concentrations, the computed voltages are certainly very underestimated. This underestimation can be very clearly seen at very low Na concentrations (<15%, shown by a broken line in Fig. 3).

Fig.3 also allows comparison with previously obtained results by Toumar et al.[8] One can see a general agreement with our calculations, particularly at high Na concentrations. It

should be noted that although FM ordering was probably imposed in calculations of Toumar et al for all studied Na concentrations (this aspect was not clarified in their work), our calculations for AFM tend to give nearly the same voltage profile for high Na concentrations. Moreover, our own estimate of the voltage, assuming FM ordering for high Na concentrations (>50%) indicates a presence of three plateaux with voltages 2.45V (from 100% to 75% Na concentration), 2.51V (from 75% to 66.66%) and 2.60V (from 66.66% to 50%). These values are also in a close agreement with the results of Toumar el at for this Na concentration range and our calculations for the case of AFM ordering, which is more favorable at these Na concentrations (Fig. 3).

Given a small difference in computed voltage values, we find that assumption of FM ordering seems to be acceptable, at least for evaluation of voltage profile of $NaMnO_2$, in spite of higher energies for FM configurations at high Na concentrations (Fig. 4). We however need to stress that this aspect still needed to be tested, in spite of a higher computational cost associated with evaluation of total energies of the cells with AFM ordering. One should also be mindful that the impact of a change of magnetic ordering might be more pronounced for voltage profiles of other magnetic materials, requiring to address this issue using the approaches as the one we adopted in this work. Moreover, this aspect could be very crucial when comparing stability of various competing phases at different Na concentrations.

3.2 The voltage profile with U parameters, evaluated using LR

We applied self-consistent evaluation of U parameters for configurations that have been found to have the lowest energies using the DFT+U approach with a fixed value of U (U=4eV) for each studied Na concentration. In Fig. 4 (top) we present the computed value of U as a function of Na concentration. We find that U increases for lower Na concentrations, which corresponds to transformation of a larger percentage of Mn^{3+} in Na_xMnO_2 into Mn^{4+} cations upon desodiation. In Fig. 4 we have also indicted the value of U chosen by Toumar et al using a fitting approach[8] by a broken horizontal line which stretches across the entire

Na concentration range. Clearly our calculated values of U are all reasonably close to the value obtained by the fitting procedure, indicating that calculations based on linear response are expected to be in a general qualitative agreement with those, performed using fitting approach.

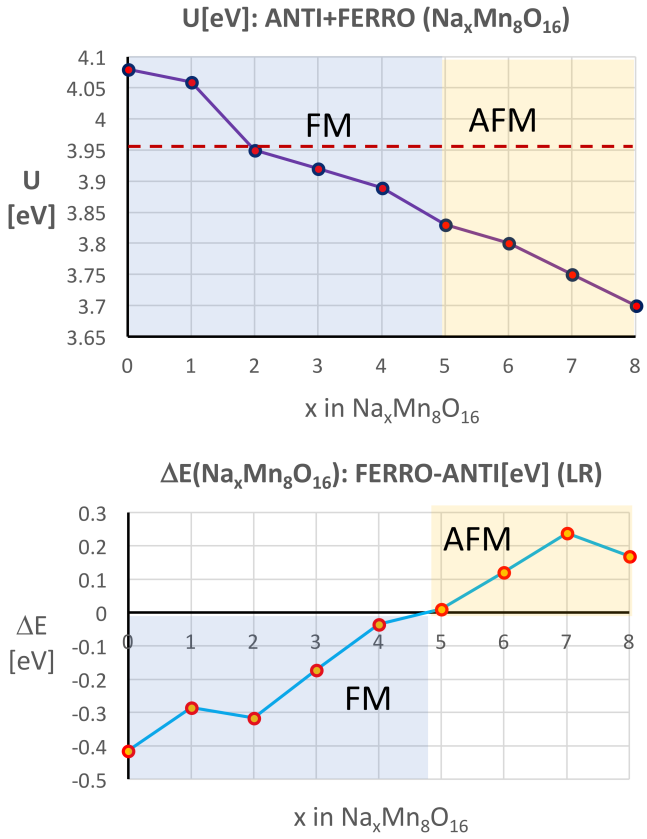

Figure 4: The U parameters evaluated using LR calculations; The value adopted in paper of Toumar et al[8] is indicated by the broken line (top); The ΔE, defined by eq. (2), showing concentrations where FM or AFM ordering is more favorable (bottom).

Similar to the discussion in the previous Section, we have analysed stability of magnetic ordering as a function of Na concentration, using the calculations with U parameters shown in Fig. 4 (top). Fig.4 (bottom) provides a respective graph which shows very similar trend as compared to the results of calculations performed using a fixed value of U (given in Fig. 2). Namely, here we also find that AFM ordering prevails at high Na concentrations (above 62.5%), whereas FM is more preferential when more Na cations are extracted (below 62.5%). Similar to the calculations of voltages with fixed value of U, we employ magnetic ordering,

which corresponds to the ground state at each specific Na concentration.

Now we proceed to discussion of a voltage profile, computed using LR parameterisation of DFT+U calculations (Fig.3, bottom). Calculations reveal that at high Na concentrations (62.5% and above), the voltage values are nearly constant, with respective value slightly higher than in the case of calculations with fitted U (2.7V vs. 2.5V as obtained with U=4eV). This value is in a better agreement with the results of measurements of the first cycle, however it is slightly higher if comparison is made with subsequent cycles (the measured voltage is about 2.5V[7]). The other difference with the computations at fixed value of U is a pronounced voltage step at Na concentration of 62.5%, predicted when linear response parameterisation is used (Fig. 3). We should point out that the voltage step at this specific concentration indicates a strongly stabilised structure with $Na_5Mn_8O_{16}$ stoichiometry. The structure with this stoichiometry was found exceptionally stable in combined experimental and theoretical work of Li et al.[28] However, in case of calculations with fixed U parameter, no voltage step is predicted at this Na concentration (calculations of Toumar et al predicted a very small step at this concentration, only weakly visible in their presented plot of calculated voltages[8]), indicating no special stability of a structure with $Na_5Mn_8O_{16}$ stoichiometry, in contrast to the calculations with LR parameterised U. We shall re-address this observation further in Section 5, where we discuss several identified partially desodiated configurations including the one with $Na_5Mn_8O_{16}$ stoichiometry.

Similar to calculations with the fixed value of U, we find that computed voltage increases when Na concentration drops below 62.5%, in agreement with experimental measurements. The key difference however is that computed values are higher in case of LR parameterization and definitely closer to the experimentally measured deintercalation curve, as compared to calculations with a fixed value of U. Moreover, for very low Na concentrations (below 15%) the LR parameterised calculations predict substantially higher values of voltage (which is however averaged over a wide concentration range) also in a better agreement with experiment (Fig. 3). To further quantify a comparison between abilities of discussed

computational approaches to reproduce experimental voltage profile, we refer the reader to Supporting Material Section.

We also wish to comment about greater predicted stability of a structure with $Na_5Mn_8O_{16}$ stoichiometry and higher predicted voltages at low Na concentrations when LR parameterisation is used from numerical viewpoint. It is clear from the Fig. 4 that the value of U parameter at 62.5% Na concentration is located slightly below the nearly straight line, formed by U parameters in the range of 50-100% of Na concentrations. As a smaller value of U leads to lower values of a total energy of the same configuration, the calculations parameterised by LR predict greater stability of a structure at this Na concentration as compared to calculations with the fixed U parameter. In a similar vein, the relatively large values of U parameter at low Na concentrations (0% and 12.5%), which lie above the nearly straight line of U as a function of Na concentration in the interval from 50% to 25%, can also explain high values of total energies of the respective structures with very low Na concentrations. These large values of U also account for higher predicted voltages upon complete Na removal as compared to calculations with a fixed value of U, resulting in a better agreement with experimental measurements.

With respect to the general trend of close to linear increase of U with Na removal, we need to note that such dependence also causes higher predicted voltages as compared to calculations with the same U parameter (assuming that the same structures are used in these calculations). Indeed, if the larger value of U is used for more desodiated structure in eq. (1), the total energy of this structure with lower Na concentration is higher as compared to the calculations with a fixed U, thus resulting in higher predicted voltages. This higher voltages, obtained with DFT+U calculations parameterised with LR method are however numerically closer to the experimental measurements as compared to calculations with fixed U which predict underestimated voltages.

4. Results: electronic, magnetic and structural properties of studied structures

4.1 $NaMnO_2$ and MnO_2 configurations and the role of oxygen in redox steps

We start from comparison between AFM and FM ordering for fully sodiated $NaMnO_2$ structure. In Fig. 5 we provide PDOS of Mn cations (3+ oxidation state) and oxygen anions for both spin channels. For both types of magnetic ordering DFT+U calculations predict an insulating character for $NaMnO_2$. It is obvious that not only Mn^{3+} cations have very different PDOS of majority and minority channels, but oxygen anions also have non-equal majority and minority PDOS even for this case of fully stoichiometric and defect-free structure. A clear difference between the AFM and FM ordering could be seen in PDOS of oxygens, particularly in minority channels: in case of FM ordering, the PDOS of minority channel falls into a narrower energy range as compared to PDOS of majority channel (the width of spin down channels are indicated by the broken lines in Fig. 5). This is different from AFM ordering where PDOS of minority channel of oxygens lies in a wider energy range with relatively low values at higher energies (about 1-1.5eV below Fermi level).

To characterise the degree of localisation of electronic states on Mn and O, we have also evaluated the projections of occupied bands on d and p orbitals in the respective atomic spheres. Table 1 provides the calculated charges, where for AFM ordering we present calculations for Mn cation with positive magnetic moment and for oxygen anion with negative magnetic moment. Our calculations reveal that total charges (given as the number of electrons) in majority and minority channels of Mn are very similar for AFM and FM ordering (Table 1). There is only a slightly larger minority charge in AFM as compared to FM ordering, whereas reverse occurs for majority charges. For oxygens in case of AFM ordering there are slightly greater charges in minority channels as can be seen from Table 1, whereas

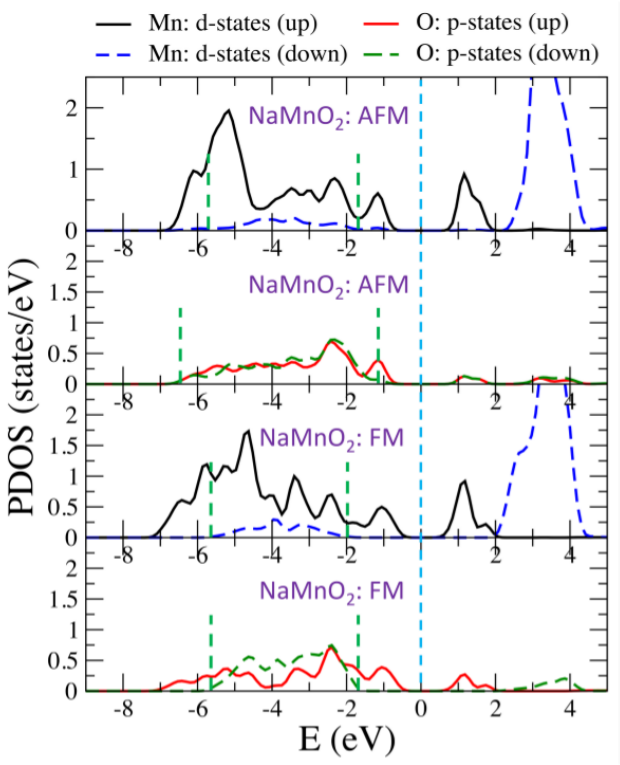

Figure 5: The PDOS for Mn and oxygens of $NaMnO_2$. The Fermi level is indicted by the blue broken line and is set to zero. The width of minority channels of Mn and oxygens are indicted by the green broken lines.

for FM ordering the charges are almost the same in spite of clearly different PDOS for two spin channels as can be seen in Fig.5.

Table 1: The charges, localised in atomic spheres, calculated for spin up and spin down channels.

	charges of spin up/down channels				
Material	Mn (AFM)	Mn (FM)	O (AFM)	O (FM)	U (AFM/FM)
$NaMnO_2$	4.318/0.529	4.324/0.515	1.730/1.763	1.745/1.748	3.70/3.65
MnO_2	3.984/0.844	4.036/0.783	1.694/1.740	1.632/1.798	4.06/4.08

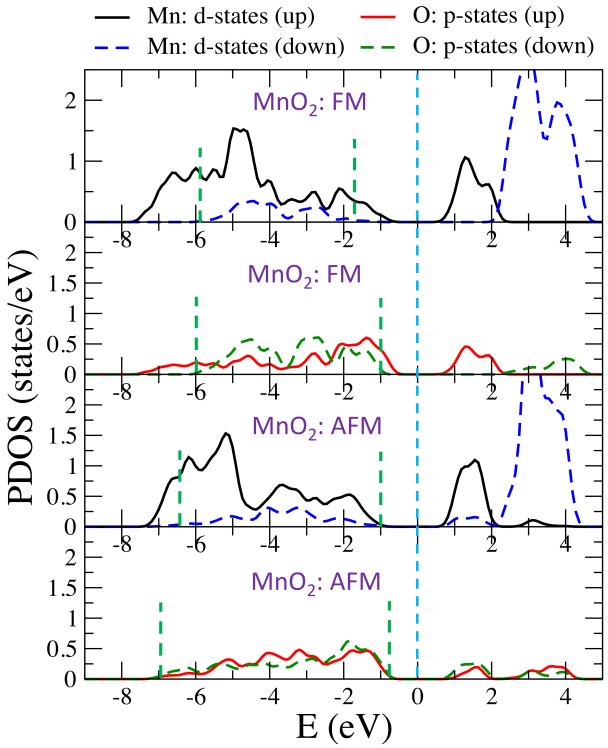

Figure 6: The PDOS for Mn and oxygens of MnO_2. The Fermi level is indicted by the blue broken line and is set to zero. The width of minority channels of Mn and oxygens are indicted by the green broken lines.

Now we proceed to discussion of MnO_2. The PDOS of Mn and O of MnO_2 for both types of magnetic ordering are provided in Fig.6. We note that calculations predict that fully desodiated material is also an insulator with the bandgap, similar in value to the fully sodiated $NaMnO_2$ structure. The total charges of majority and minority spin channels of

Mn^{4+} cations of MnO_2 are different from respective values for Mn^{3+} of $NaMnO_2$ as can be seen from Table 1. Indeed, we find that the charge of majority channel decreases upon desodiation with concomitant increase of the charge in minority channel (Table 1). These changes in the amounts of charges of majority and minority channels account for the change of magnetic moment of Mn upon oxidation step $Mn^{3+} \rightarrow Mn^{4+}$ (the absolute value of Mn moment decreases). We also find that oxygen anions are spin polarized for both types of magnetic ordering in MnO_2. Additionally, in case of FM ordering, magnetic moments on all oxygens are negative, whereas magnetic moments on Mn are all set positive. Based on Table 1 it is clear that upon Na removal and complete desodiation of $NaMnO_2$ structure, the charge in minority channel of oxygens increases with concomitant decrease of majority charge (relative to nearly equal values for fully sodiated case).

The Bader charges on Mn and oxygens upon Na removal have been also evaluated for the entire range of Na concentrations as is shown in Fig. 7 (the values of Bader charges are averaged over all respective atoms of computational cells). It is clear that for both Mn and O the Bader charges tend to decrease with Na removal. For Mn however, the Bader charges are found to be nearly constant for 62.5% and 50% of Na concentrations as well as for 12.5% and 25%. On the other hand, for oxygens we find that Bader charges decrease with Na content nearly linearly for entire concentration range. These trends of atomic charge dependence from Na amount can not explain the voltage character, namely close to constant voltage values for high Na concentrations (>62.5%) and steady voltage increase upon Na removal for lower Na concentrations (<62.5%).

In addition to the charge analysis, we have also evaluated magnetic moments on Mn and O at various Na concentrations. The absolute values of magnetic moments of Mn and oxygens have been summed up and averaged to obtain a characteristic magnetic moment at a specific Na concentration, as is shown in Fig. 8. We find the absolute values of magnetic moments of Mn decrease nearly linearly with Na concentration. However, for oxygens we find a sharp change of magnetic moments when Na concentration drops below 62.5% of Na

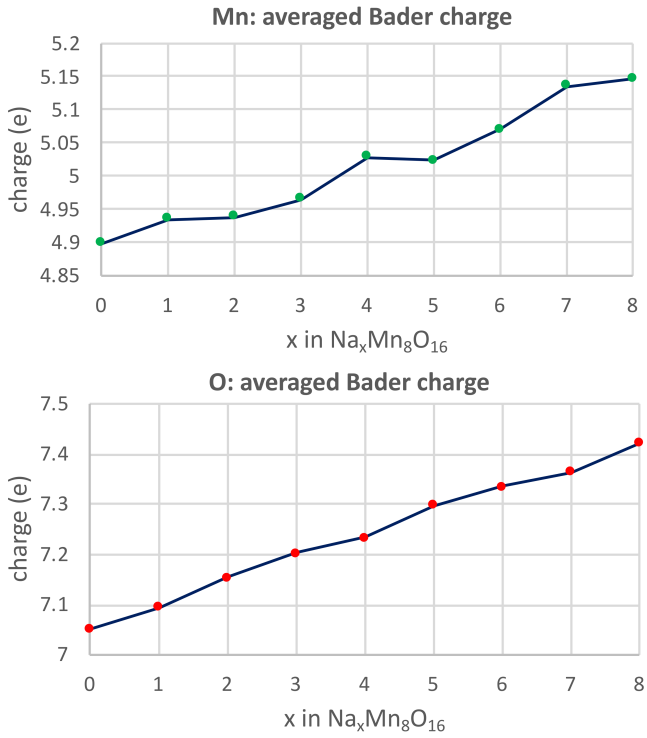

Figure 7: The Bader charges on Mn and oxygens (averaged over all respective atoms in the computational cell) as the functions of concentration of Na.

(Fig. 8). This is an indication that evolution of magnetic moments of oxygen seems to be the factor which affects the voltage character of $NaMnO_2$, as the dependence of magnetic moments from concentration mimics the changes in computed and experimentally observed voltage profiles (Fig. 3).

4.2 Analysis of partially desodiated Na_xMnO_2 structures

We find that all identified partially desodiated ground states possess highly ordered arrangements of Na. This finding is in a general agreement with previous computational works [8,47] who also observed a high ordering of Na cations in optimised ground state configurations. Moreover, as Na removal results in Mn oxidation, herein we discuss the ordering of Mn^{3+} and Mn^{4+} cations, as these also strongly influence the energetics and stability of studied atomic models.

In order to clarify a connection between Mn oxidation and Na removal, we need to

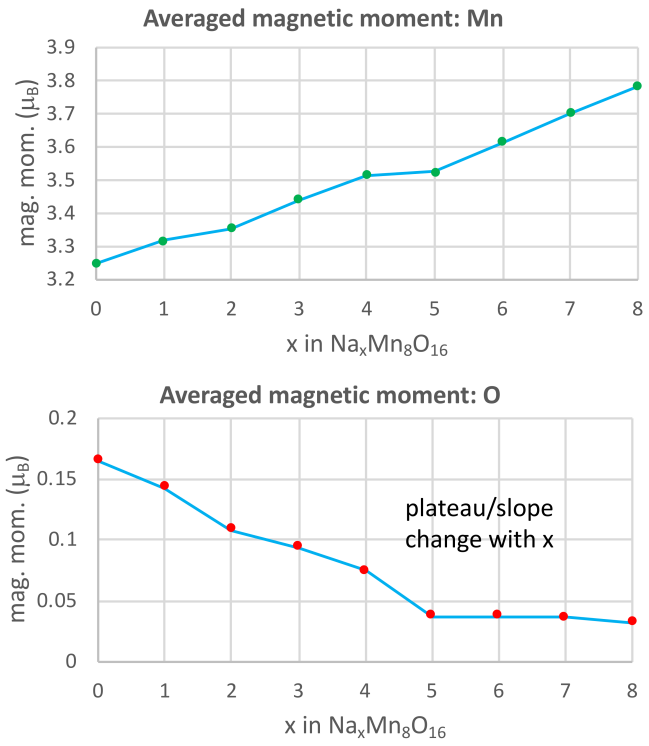

Figure 8: The averaged absolute magnetic moments of Mn and oxygens as the functions of Na concentration.

elucidate structural transformation steps, which occur after formation of a Na vacancy. The structure of $NaMnO_2$ prior to Na removal is shown in Fig. 9 (left). The Mn cations and their closer neighbours form elongated chains as is shown in Fig. 9 (Mn-O chains) and such chains are aggregated into planes, highlighted by the orange color in Fig. 9. A Mn cation forms shorter bonds with four neighboring oxygens and longer bonds with two other oxygens as is indicted by the broken lines in Fig. 9 (left, 1.96Å for bonds within the plane and 2.43Å for the inter-plane Mn-O bond). Removal of a Na cation results in oxidation of Mn which is accompanied by lifting of Jahn-Teller distortions via shortening of Mn-O bonds (Fig. 9, right). The bonds that are shortened most significantly are the longer inter-plane Mn-O bonds of an oxidised Mn^{3+} cation prior to oxidation. We find that removal of Na also results in shifting of an oxygen in the plane adjacent to the removed Na towards Mn cation which is oxidised (for $Na_7Mn_8O_{16}$ the inter-plane bond length of the Mn^{4+} is shorten to 2.01Å as is shown in Fig. 9, right). The introduced Na vacancy, shifted oxygen and the oxidised Mn^{4+} cation are located in three adjacent planes (highlighted by the orange color in Fig. 9). This observation allows to elucidate the connection between the location of Na vacancies and oxidised Mn^{4+} cations.

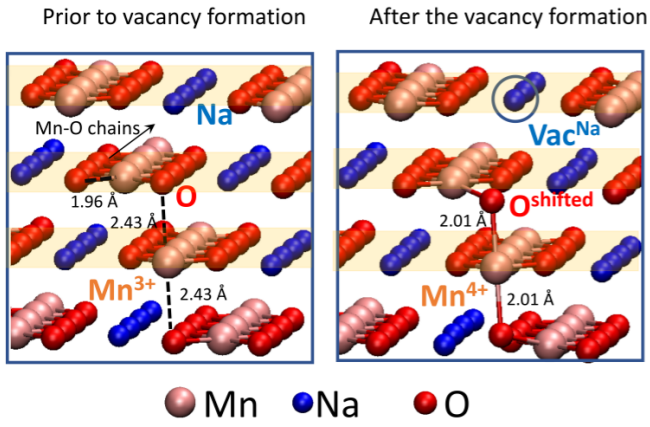

Figure 9: Lifting of Jahn-Teller distortions via removal of a Na cation and oxidising Mn^{3+} into Mn^{4+}. The Mn-O chains are indicated and the atomic planes are highlighted by orange color. The shorter in-plane bond (1.96Å) and longer inter-plane bond (2.43Å) are indicated on the left. The short inter-plane bonds (2.01Å) of an oxidised Mn^{4+} are indicted on the right.

Upon establishing the mechanism of structural changes, caused by Na vacancy formation and subsequent Mn oxidation, we proceed to analysis of structural properties of ground state structures at Na concentrations which give rise to the steps of voltage profile in Fig. 3. The six structures are shown in Fig.10, where we highlighted Mn^{3+} and Mn^{4+} by different colors (colors for Na and O are provided in Fig. 9). We present the structures using the same perspective as in Fig. 9 to highlight the link between the lifting of Jahn-Teller distortions for oxidised Mn^{4+} cations and formation of Na vacancies.

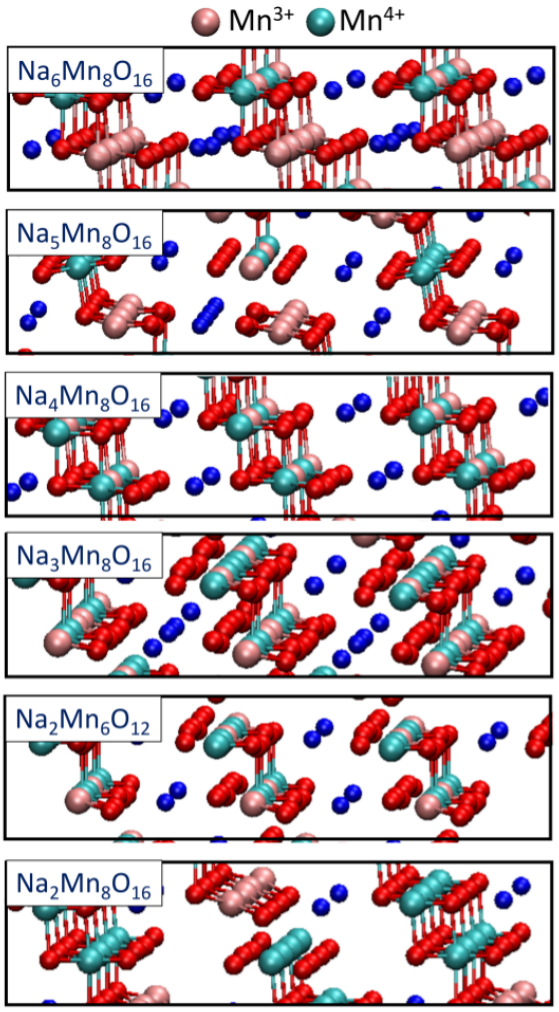

Figure 10: The ground state structures at all studied Na concentrations.

Using Fig. 10 we wish to point out on one interesting property of two ground state structures, namely $Na_5Mn_8O_{16}$ and $Na_2Mn_8O_{16}$, which contain the chains of Mn cations in

either 3+ or 4+ oxidation states. The presence of two types of chains elongated in the same direction, which contain only Mn^{3+} or Mn^{4+} cations might be considered counterintuitive for the low energy configuration in view of generally different atomic radii for a cation in different oxidation states. As a possible explanation we should note that the lengths of Mn-O bonds in the discussed planes (Fig. 10) change only marginally upon Na removal, whereas the most pronounced structural changes are associated with shortening of inter-plane Mn-O bonds upon Mn oxidation in Fig. 10. Indeed, even a simple analysis of fully sodiated and desodiated structures show that in-plane Mn-O bonds differ only slightly in bond length: 1.96Å for $NaMnO_2$ and 1.94Å for MnO_2, explaining the presence of Mn^{4+} and Mn^{3+} chains in low energy structures.

On the other hand, several ground state structures, particularly with intermediate Na concentration ($Na_4Mn_8O_{16}$, $Na_3Mn_8O_{16}$, $Na_2Mn_6O_{12}$) contain the chains of Mn cations in different oxidation states (Mn^{3+} or Mn^{4+}), which are periodically repeated. Particularly, $Na_4Mn_8O_{16}$ configuration contains the chains with alternating Mn^{3+} and Mn^{4+} cations in all planes, which corresponds to uniform distribution of Mn with two oxidation states and uniform distribution of Na and their vacancies.

In view of a clear correlation between the adopted oxidation states of Mn cations and structural properties of the desodiated phases, we monitored the averaged Mn-O bond lengths at various Na concentrations. In Fig. 11 we present the averaged bond lengths for Mn^{3+} and Mn^{4+}, obtained as a mean value of all Mn-O bonds of Mn cations, averaged over all Mn for each of the oxidation state. In addition, in Fig. 11 we also provide averaged bond lengths, which however are calculated as a mean value of Mn-O inter-plane bonds (two inter-plane bonds per each Mn cation).

Fig.11 clearly indicates that structural changes are unlikely to be the factor, which can account for a change of voltage curve from plateau to slope (Fig. 3). Indeed, the bond length for Mn^{3+} cations is largely a monotonic function with some oscillations at low Na concentrations. At a first glance it seems possible that transformation of averaged bond

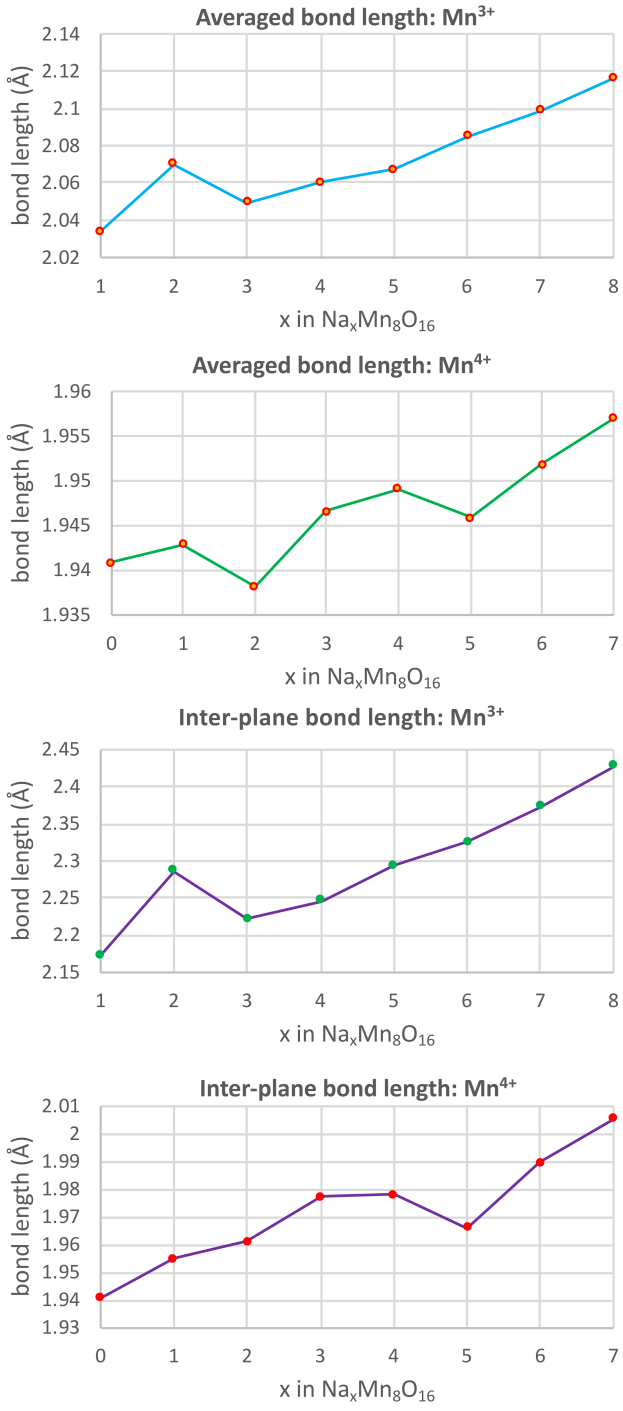

Figure 11: The averaged Mn-O bond lengths for Mn^{3+} and Mn^{4+} as the functions of Na concentration. The averaged inter-plane bonds are also provided below.

length for Mn^{4+} cation might provide some explanation of the voltage change with Na concentration, for instance due to increases upon lowering of Na concentration from 62.5 down to 50% (Fig. 11). This change however is very small (only about 0.01Å for inter-plane bonds) making this factor very weakly responsible for the change of the voltage character. In addition to the bond length analysis, we also present the dependence of the lattice constant, which characterises the distance between the O-Mn-O trilayers, shown in Fig. 12. We find that in spite of Na removal, this lattice constant could also increase for some concentrations, dropping significantly only in case of MnO_2.

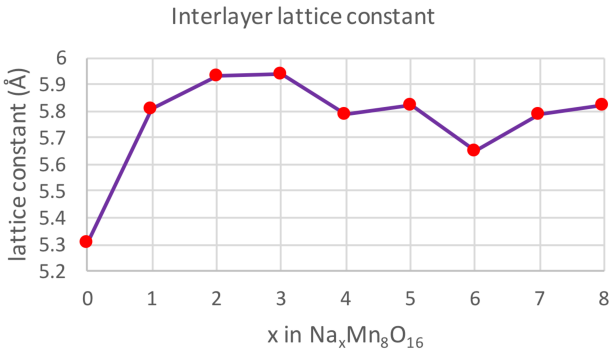

Figure 12: The lattice constant, which characterises the distance between O-Mn-O trilayers as a function of Na concentration.

Therefore our analysis of structural, electronic and magnetic properties shows that only evolution of magnetic moments could be key factor responsible for the voltage change from plateau to slope upon Na removal.

5. Results: comparison with previously identified structures

Several partially desodiated structures have been identified and studied recently using experimental and theoretical approaches.[28,29] It is of interest to compare these structures and their properties with the ground state configurations obtained within this study, as we discuss below.

5.1 The $Na_{5/8}MnO_2$ model

In 2014 Li et al reported the $Na_{5/8}MnO_2$ model, derived via analysis of XRD and STEM images.[28] In addition, exhaustive computational study of a large number of various structural candidates (300 configurations) also confirmed that this experimentally identified model indeed has the lowest energy[28] (to perform these computations, Li et al relied on DFT+U method in Dudarev's formulation,[32] employed for correction of the same PBE functional,[31] which we also adopt herein). Using computational analysis, Li et al have found that Na vacancies are arranged in such a way that three types of stripes of cations are formed in the atomic planes of studied crystal: Mn^{3+}, Mn^{4+} and Mn^{3+}/Mn^{4+} alternating cations. DFT+U calculations have also allowed to determine that the magnetic ordering of the stripes, formed by Mn^{3+}, Mn^{4+} and Mn^{3+}/Mn^{4+} alternating cations are AFM, ferrimagnetic and also ferrimagnetic respectively.[28] In Fig. 13 we provided the optimised structure, obtained using the set of coordinates provided by Li et al. We indicted the stripes of Mn^{3+}, Mn^{4+} and Mn^{3+}/Mn^{4+} all in agreement with the description provided by Li et al (the same type of magnetic ordering is also introduced in our calculations).

In Fig. 13 we also provide a visual comparison between the model, reported by Li et al[28] with the structure, obtained herein as a ground state for 62.5% Na concentration. A very close structural resemblance is obvious between these two configurations. The only difference between the two models is the ordering of Mn^{3+}/Mn^{4+} cations: every other chain of the model of Li et al is arranged in a changed order of Mn^{3+} and Mn^{4+} cations (Mn^{3+}/Mn^{4+} as compared to adjacent Mn^{4+}/Mn^{3+}) in contrast to our derived structure, where all chains have Mn^{3+}/Mn^{4+} alternating order. This small structural difference leads to only a very little difference in total energy: our model is found by 0.1 eV more stable in case if the same U parameter (3.83eV) is employed for calculations of large computational cells ($Na_{20}Mn_{32}O_{64}$ unit). However, when LR parameterisation is applied, we find that the model of Li et al has a slightly smaller calculated value of U parameter (3.81 eV), which technically results in a slightly higher stability of a model, described in ref. 28 (by 0.3eV for $Na_{20}Mn_{32}O_{64}$ cells).

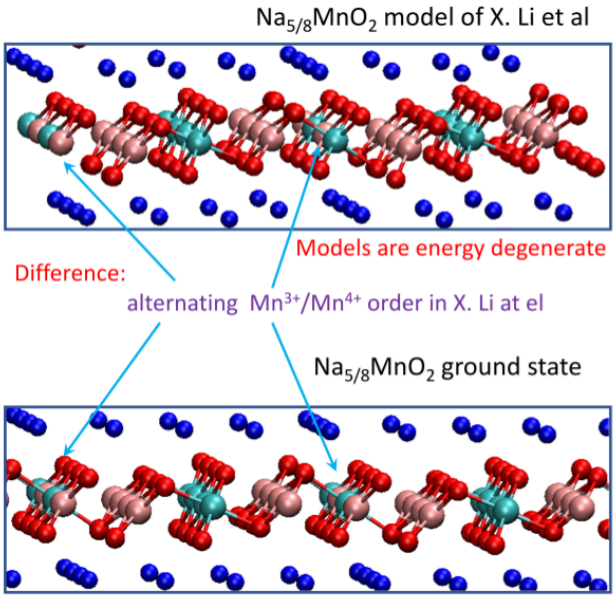

Figure 13: The $Na_{5/8}MnO_2$ structure proposed by Li et al (top) with highlighted Mn^{3+} and Mn^{4+} cations. For comparison, our optimised structure with the same stoichiometry is provided below. The key structural difference between the two models is also indicated.

However, given a very small difference of U parameters, calculated for these two models with the same Na concentration, it seems reasonable to assume that these two structures are degenerate in energy (a very marginal difference in total energy leads only to a very small change of the calculated voltage profile in Fig. 3). Thus we find that our obtained model is nearly identical to the model, obtained by Li et al and both of them correspond to the ground state structure at 62.5% of Na concentration.

Nearly identical energies of the two models also lead to the conclusion that the structure proposed by Li et al does not give rise to a voltage step, when a fixed value of U is employed (Fig. 3). This means for instance that combinations of the structures, obtained for 50% of Na concentration and at 67.5% of Na should provide more stable configuration at 62.5% of Na concentrations, thus ruling out a possibility of a distinct ground state for the discussed $Na_{5/8}MnO_8$ model. On the other hand, using calculations performed employing U parameters, obtained via LR parameterisation, we find that both models (which possess nearly the same energy) give rise to a pronounced voltage step, thus explaining their presence and

experimental observation in partially desodiated structures with Na concentrations above 50%.[28]

We also need to comment about magnetic properties of the structures with 62.5% concentration of Na. We find that the difference in total energies for FM and AFM ordering for $Na_{20}Mn_{32}O_{64}$ cells is only 0.03eV. However, it should be emphasized that this difference is sensitive to the employed value of U parameter. For instance, for the model of Li et al we find that AFM ordering is by 0.4eV more favorable than FM ordering if smaller value of U=2.47eV is employed.[28] However, such a low value of U is not acceptable for evaluation of a voltage profile using a fixed value of U. Indeed, as we have mentioned above (Section 3.1), even when a larger value of U=3.95eV is employed, the computed voltages tend to be underestimated, particularly for low Na concentrations.

5.2 The $Na_{1/2}MnO_2$ and $Na_{1/3}MnO_2$ models

Recently Chen et al performed a detailed analysis of partially desodiated Na_xMnO_2.[29] Using XRD and TEM methods, they identified several configurations at Na concentrations of 62.5, 50, 33 and 5.55%. Analysing the identified structures, Chen et al made an observation that Na cations and Na vacancies aggregate on the separate planes, cutting across the layers of Na_xMnO_2. This aggregation of Na and their vacancies into these special planes has been termed as "supercharge separation".[29] The observations of Chen et al are in general agreement with our analysis in Sec. 4.2 where we have pointed out that strings of Mn^{3+} and Mn^{4+} occupy the planes, bonded by relatively long Mn-O bonds, particularly at high Na concentrations (see Fig. 10). In the following we provide a comparison between the structures, characterised by Chen et al and the ground states at the same concentrations, obtained within our work.

The structure at 62.5% Na concentration, characterised experimentally by Chen et al is identical to the model, proposed by Li et al.[29] Thus, for this concentration of Na, the work of Chen et al confirms the findings of Li et al with regard to exceptional stability of this

configuration. On the other hand, the model at 50% of Na was found to be different from the one, reported in the work of Toumar et al[8] as well as from our work. Comparison shows that the structure, identified by Chen et al differs from our model by the arrangement of Mn^{3+} and Mn^{4+} cations, as can be seen in Fig.14 (the respective coordinates for the model of Toumar et al are not available to the best of our knowledge). In spite of a slightly smaller U parameter, obtained for the structure of Chen et al as compared to the ground state, found in our study (3.87 vs. 3.89 respectively), we find that the latter is a more favorable structure (by 0.18eV for a $Na_4Mn_8O_{16}$ unit). We should also note that our calculations reveal that FM ordering is more favorable for the model of Chen et al than possible AFM configurations, which we have tested. With regard to configuration at 33% of Na concentration, we find that our proposed ground state coincides with the one, observed by Chen et al and also proposed by Toumar et al in their computational study. Thus only the configuration at 50% Na concentration is somewhat different from experimental observations of Chen (similarly to the model of Toumer et al who also predicted different model for this case[29]).

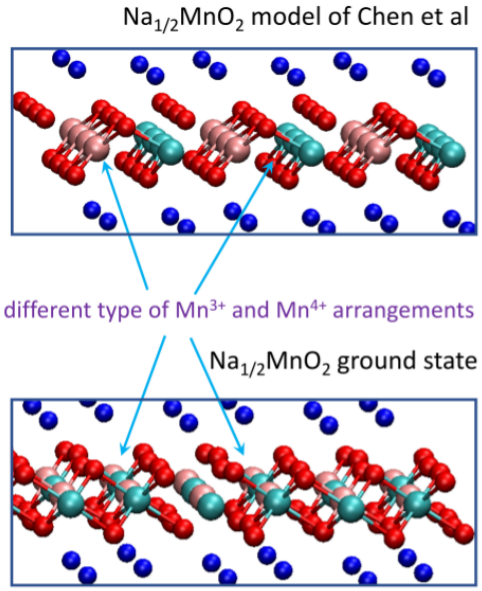

Figure 14: The $Na_{1/2}MnO_2$ structure proposed by Chen et al (top) with highlighted Mn^{3+} and Mn^{4+} cations. For comparison, our optimised structure with the same stoichiometry is provided below. The key structural difference between the two models is also indicated.

The XRD measurements of Chen et al have also revealed transformation of O3 into O1 structure upon Na removal at low Na concentrations (<25%).[29] Particularly in the limit of a complete Na removal, experimental measurements indicate that O3 structure is fully transformed into O1.[29] We have performed a calculation of fully desodiated O1 MnO_2 configuration using DFT+U calculations. As in other cases of the models with the same Na concentration, we find that the U parameters are nearly identical for fully desodiated MnO_2 in O1 and O3 polymorphs. Our calculations show that O3 phase is slightly more favorable as compared to O1 arrangement. Thus DFT+U calculations do not predict a preference of O1 over O3 as is found experimentally. We should note that this inability of DFT+U approach to provide a distinct preference of one phase over the other in accordance with experimental observations has been also reported in the previous studies.[10]

The work of Chen et al have also provided the experimentally determined lattice constants in the case of low Na concentrations. In a completely desodiated case, the measured interlayer lattice constant of 4.5 Å has been reported.[29] This value however is lower than the one obtained by DFT+U calculations, (5.1Å, according to our calculations for O1 model). Such overestimation of interlayer distances by DFT+U calculations is common for layered oxides in view of the absence of proper treatment of van der Waals interactions that are required to account for a stronger binding between the layers. To test this, we have applied D3 van der Waals corrections to our DFT+U calculations,[48] which resulted in a smaller interlayer lattice constant of 4.6 Å in a better agreement with the measurements of Chen et al.

A special comment should be made about estimation of voltages when D3 corrections are added to DFT+U calculations, particularly in view of the need to re-adjust the employed U parameters, taken for instance from the Materials Project database[49] as these have been obtained via fitting of the results of PBE calculations free from discussed corrections.[50] Another important aspect is the treatment of a Na metal cell, required for voltage calculations using eq. (1). It is known that application of van der Waals corrections for analysis of alkali metals (e.g. bcc Li or Na) results in a very poor description of electronic structure,[51] questioning

reliability of this approach. In this regard we should point out to a new method which has been proposed recently, holding a promise for adequate description of oxide materials and pure alkali metals via DFT method with van der Waals corrections.[52]

In the Supporting Material Section we provide our preliminary results of evaluation of voltage profiles using additional D3 corrections. As could be seen from Fig. S3, further work is needed to calculate the voltage in a better agreement with experiment (see Supporting Material Section for a discussion of a possible simple shortcut, which could be used for accurate evaluation of voltages and lattice parameters).

5. Conclusions

In this work we have demonstrated that DFT+U calculations parameterised by the LR method can be used for calculation of a complex voltage profile of a cathode material even if dependence of magnetic ordering of transition metal cations from Na concentration is taken into account. Our calculations show a good agreement with experimental measurements, particularly for low Na concentrations, where calculations with the fixed value of U parameter, obtained via a fitting procedure, provided underestimated values (Fig. 3).

In addition, we have also analysed the change of structural, electronic and magnetic properties of Na_xMnO_2 upon deintercalation. Our analysis revealed that the change of a voltage dependence from plateau to a constant increase upon Na removal is best described by the increase of absolute values of magnetic moments of oxygen anions (Fig. 8), rather than changes of Bader changes on Mn and O, evolution of bond lengths of Mn^{3+} and Mn^{4+} cations and even magnetic moments of Mn.

We have also discussed the recently identified structures of partially desodiated Na_xMnO_2,[28,29] particularly how these are featured in the calculated voltage profile. Our calculations show that linear response parameterisation provides U parameters, which allow to predict the presence of the voltage steps right at the concentrations, which correspond to experimen-

tally identified configurations. This is in contrast to calculations with the fixed value of U parameter, which for instance do not predict relative stability of the $Na_{5/8}MnO_2$ configuration,[28] identified experimentally, due to the absence of any pronounced step in the computed voltage profile (Fig. 3). Additionally, our calculations predicted a $Na_{1/3}MnO_2$ configuration in full agreement with experimental analysis of Chen et al[29] and previous calculations of Toumar et al.[8] On the other hand, the $Na_{1/2}MnO_2$ model, reported by Chen et al differs from our ground state structure with the same stoichiometry (similarly, Toumar et al also provided a different configuration for this concentration). Our calculations however predict a lower energy for our proposed model in spite of a disagreement with experimental assignment by Chen et al.

In summary the discussed computational approach can be used for accurate evaluation of voltage profiles of materials, requiring no experimental fitting. It is possible however that the accuracy may be dependent on the ability of the employed DFT+U method to reproduce other properties of studied materials, such as magnetic moments of constituent TM cations,[53] etc. Other possible limitations of presented method can be associated with less accurate evaluation of structural properties of layered materials at low Na concentrations.

Supporting Information Available

Selection of k-point mech; construction of partially desolated cells; convex hull evaluation for FM and AMF ordering; quantitative comparison of accuracy of the methods used for voltage calculation; voltage profile calculated with van der Waals corrected functional

Acknowledgement

M. Shishkin acknowledges financial support from Grant-in-Aid for Scientific Research (C) 18K05031 (Japan Society for the Promotion of Science (JSPS)). This work was performed under the management of Elements Strategy Initiative for Catalysts and Batteries (ESICB).

References

(1) Myung, S.-T.; Maglia, F.; Park, K.-J.; Yoon, C. S.; Lamp, P.; Kim, S.-J.; ; Sun, Y.-K. Nickel-Rich Layered Cathode Materials for Automotive Lithium-Ion Batteries: Achievements and Perspectives. *ACS Energy Letters* **2017**, *2*, 196–223.

(2) Hu, Y.-S.; Komaba, S.; Forsyth,; Johnson, C.; Rojo, T. A New Emerging Technology: Na-Ion Batteries. *Small Methods* **2019**, *3*, 1900184.

(3) Wang, S.; Sun, C.; Wang, N.; Zhang, Q. Ni- and/or Mn-based layered transition metal oxides as cathode materials for sodium ion batteries: status, challenges and countermeasures. *Mater. Chem. A* **2019**, *7*, 10138.

(4) Kubota, K.; Kumakura, S.; Yoda, Y.; Kuroki, K.; Komaba, S. Electrochemistry and Solid-State Chemistry of NaMeO2 (Me = 3d Transition Metals). *Adv. Energy Mater.* **2018**, *8*, 1703415.

(5) Mariyappan, S.; Wang, Q.; Tarascon, J. M. Will Sodium Layered Oxides Ever Be Competitive for Sodium Ion Battery Applications? *Journal of The Electrochemical Society* **2018**, *16*, A3714.

(6) Delmas, C.; Fouassier, C.; Hagenmuller, P. Structural classification and properties of the layered oxides. *Physica B* **1980**, *99*, 81–85.

(7) Ma, X.; Chen, H.; Ceder, G. Electrochemical Properties of Monoclinic $NaMnO_2$. *J. of Electrochem. Soc.* **2011**, *158*, A1307–A1312.

(8) Toumar, A. J.; Ong, S. P.; Richards, W. D.; Dacek, S.; Ceder, G. Vacancy Ordering in O3-Type Layered Metal Oxide Sodium-Ion Battery Cathodes. *Phys. Rev. Appl.* **2015**, *4*, 064002.

(9) Zhang, R.; Lub, Z.; Yanga, Y.; Shi, W. First-principles investigation of the monoclinic

$NaMnO_2$ cathode material for rechargeable Na-ion batteries. *Current Applied Physics* **2018**, *18*, 1431.

(10) Kaufman, J. L.; der Ven, A. V. Na_xCoO_2 phase stability and hierarchical orderings in the O3/P3 structure family. *Phys. Rev. Mater.* **2019**, *3*, 015402.

(11) Anisimov, V.; Izyumov, Y. *Electronic Structure of Strongly Correlated Materials*, 1st ed.; Springer Series in Solid-State Sciences: New York, 2010.

(12) Anisimov, V. I.; Aryasetiawan, F.; Lichtenstein, A. I. First-principles calculations of the electronic structure and spectra of strongly correlated systems: the LDA + U method. *J. Phys.: Condens. Matter* **1997**, *9*, 767âĂŞ808.

(13) Himmetoglui, B.; Floris, A.; de Gironcolo, S.; Cococcioni, M. *Int. J. of Quantum Chem.* **2014**, *114*.

(14) Kulik, H. J. Perspective: Treating electron over-delocalization with the DFT+U method. *J. Chem. Phys.* **2015**, *142*, 240901.

(15) Wang, L.; Maxisch, T.; Ceder, G. Oxidation energies of transition metal oxides within the GGA+U framework. *Phys. Rev. B* **2006**, *73*, 195107.

(16) Saritas, K.; Fadel, E. R.; Kozinsky, B.; Grossman, J. C. Charge density and redox potential of $LiNiO_2$ using ab initio diffusion quantum Monte Carlo. *J. Phys. Chem. C* **2020**, *124*, 5893.

(17) Pickett, W. E.; Erwin, S. C.; Ethridge, E. C. Reformulation of the LDA+U method for a local-orbital basis. *Phys. Rev. B* **1998**, *58*, 1201.

(18) Zhou, F.; Cococcioni, M.; Marianetti, C. A.; Morgan, D.; Ceder, G. First-principles prediction of redox potentials in transition-metal compounds with LDA+U. *Phys. Rev. B* **2004**, *70*, 235121.

(19) Cococcioni, M.; de Gironcoli, S. Linear response approach to the calculation of the effective interaction parameters in the LDA+U method. *Phys. Rev. B* **2005**, *71*, 035105.

(20) Shishkin, M.; Sato, H. Self-consistent parametrization of DFT + U framework using linear response approach: Application to evaluation of redox potentials of battery cathodes. *Phys. Rev. B* **2016**, *93*, 085135.

(21) Timrov, I.; Marzari, N.; Cococcioni, M. Hubbard parameters from density-functional perturbation theory. *Phys. Rev. B* **2018**, *98*, 085127.

(22) Shishkin, M.; Sato, H. Theoretical Analysis of Materials, used in Energy Storage Applications: the Quest for Robust and Accurate Computational Methodologies. *The Chemical Record* **2019**, *19*, 779.

(23) Cococcioni, M.; Marzari, N. Energetics and cathode voltages of $LiMPO_4$ olivines (M=Fe, Mn) from extended Hubbard functionals. *Phys. Rev. M* **2019**, *3*, 033801.

(24) Shishkin, M.; Sato, H. DFT+U in Dudarev′s formulation with corrected interactions between the electrons with opposite spins: The form of Hamiltonian, calculation of forces, and bandgap adjustments. *J. Chem. Phys.* **2019**, *151*, 024102.

(25) Wang, J.; Wang, Y.; Seo, D.-H.; Shi, T.; S. Chen, Y. T.; Kim, H.; Ceder, G. A High-Energy NASICON-Type Cathode Material for Na-Ion Batteries. *Adv. Energy Mater.* **2020**, *10*, 1903968.

(26) Giot, M.; Chapon, L. C.; Androulakis, J.; Green, M. A.; Radaelli, P. G.; Lappas, A. Magnetoelastic Coupling and Symmetry Breaking in the Frustrated Antiferromagnet α-$NaMnO_2$. *Phys. Rev. Lett.* **2007**, *99*, 247211.

(27) Greedan, J. E.; Raju, N. P. Long Range and Short Range Magnetic Order in Orthorhombic $LiMnO_2$. *J. of Solid State Chem.* **1997**, *128*, 209–214.

(28) Li, X.; Ma, X.; Su, D.; Liu, L.; Chisnell, R.; Ong, S. P.; Chen, H.; Toumar, A.; Idrobo, J.-C.; Lei, Y.; et al, Direct visualization of the Jahn-Teller effect coupled to Na ordering in $Na_{5/8}MnO_2$. *Nature Materials* **2014**, *13*, 586.

(29) Chen, X.; Wang, Y.; Wiaderek, K.; Sang, X.; Borkiewicz, O.; Chapman, K.; LeBeau, J.; Lynn, J.; Li, X. Super Charge Separation and High Voltage Phase in Na_xMnO_2. *Adv. Funct. Mater.* **2018**, *28*, 1805105.

(30) `http://cms.mpi.univie.ac.at/vasp/vasp/vasp.html`.

(31) Perdew, J.; Burke, K.; Ernzerhof, M. Generalized Gradient Approximation Made Simple. *Phys. Rev. Lett.* **1996**, *77*, 3865.

(32) Dudarev, S. L.; Botton, G. A.; Savrasov, S. Y.; Humphreys, C. J.; Sutton, A. P. Electron-energy-loss spectra and the structural stability of nickel oxide: An LSDA+U study. *Phys. Rev. B* **1998**, *57*, 1505.

(33) Shishkin, M.; Kumakura, S.; Sato, S.; Kubota, K.; Komaba, S.; Sato, H. Unraveling the Role of Doping in Selective Stabilization of $NaMnO_2$ Polymorphs: Combined Theoretical and Experimental Study. *Chemistry of Materials* **2018**, *30*, 1257–1264.

(34) Blöchl, P. E. Projector augmented-wave method. *Phys. Rev. B* **1994**, *50*, 17953.

(35) Kresse, G.; Joubert, D. From ultrasoft pseudopotentials to the projector augmented-wave method. *Phys. Rev. B* **1999**, *59*, 1758.

(36) Monkhorst, H. J.; Pack, J. D. Special points for Brillouin-zone integrations. *Phys. Rev. B* **1976**, *13*, 5188.

(37) Parant, J.-P.; Olazcuaga, R.; Fouassier, M. D. C.; Hagenmuller, P. Sur Quelques Nouvelles Phases de Formule Na_xMnO_2 ($x \leq 1$). *J. Solid State Chem.* **1976**, *13*, 5188.

(38) Dally, R. L.; Chisnell, R.; Harriger, L.; Liu, Y.; Lynn, J. W.; ; Wilson, S. D. Thermal evolution of quasi-one-dimensional spin correlations within the anisotropic triangular lattice of α-$NaMnO_2$. *Phys. Rev. B* **2018**, *98*, 144444.

(39) Cockayne, E.; Levin, I.; Wu, H.; Llobet, A. Magnetic structure of bixbyite of α-Mn_2O_3: A combined DFT+U and neutron diffraction study. *Phys. Rev. B* **2013**, *87*, 184413.

(40) Aydinol, M. K.; Kohan, A. F.; Ceder, G.; Cho, K.; Joannopoulos, J. Ab *initio* study of lithium intercalation in metal oxides and metal dichalcogenides. *Phys. Rev. B* **1997**, *56*, 1354.

(41) `https://prisms-center.github.io/CASMcode-docs/pages/citing.html`.

(42) Thomas, J. C.; der Ven, A. V. Finite-temperature properties of strongly anharmonic and mechanically unstable crystal phases from first principles. *Phys. Rev. B* **2013**, *88*, 214111.

(43) Puchala, B.; der Ven, A. V. Thermodynamics of the Zr-O system from first-principles calculations. *Phys. Rev. B* **2013**, *88*, 094108.

(44) der Ven, A. V.; Thomas, J. C.; Xu, Q.; Bhattacharya, J. Linking the electronic structure of solids to their thermodynamic and kinetic properties. *Mathematics and Computers in Simulation* **2010**, *80*, 1393.

(45) Li, L.; Jacobs, R.; Gao, P.; Gan, L.; Wang, F.; Morgan, D.; Jin, S. Origins of Large Voltage Hysteresis in High-Energy-Density Metal Fluoride Lithium-Ion Battery Conversion Electrodes. *J. Am. Chem. Soc.* **2016**, *138*, 2838–2848.

(46) Song, B. et al. Understanding the Low-Voltage Hysteresis of Anionic Redox in $Na_2Mn_3O_7$. *Chem. Mater.* **2019**, *31*, 3756–3765.

(47) Aryanpour, M.; Miara, L.; Ryu, Y.-G. Staging and In-Plane Superstructures Formed in

Layered $NaMO_2$ M = Sc, Ti, V, Cr, Mn during Na De-Intercalation: A Computational Study. *Journal of The Electrochemical Society* **2015**, *162*, A511.

(48) Grimme, S.; Antony, J.; Ehrlich, S.; Krieg, S. A consistent and accurate ab initio parametrization of density functional dispersion correction (DFT-D) for the 94 elements H-Pu. *J. Chem. Phys.* **2010**, *132*, 154104.

(49) Jain, A.; Ong, S. P.; Hautier, G.; Chen, W.; Richards, W. D.; Dacek, S.; Cholia, S.; Gunter, D.; Skinner, D.; Ceder, G.; Persson, K. A. Commentary: The Materials Project: A materials genome approach to accelerating materials innovation. *APL Mater.* **2013**, *1*, 011002.

(50) Lozano, A.; Escribano, B.; Akhmatskaya, E.; Carrasco, J. Assessment of van der Waals inclusive density functional theory methods for layered electroactive materials. *Phys. Chem. Chem. Phys.* **2017**, *19*, 10133.

(51) Kim, W. J.; Kim, M.; Lee, E. K.; Lebegue, S.; Kim, H. Failure of Density Functional Dispersion Correction in Metallic Systems and Its Possible Solution Using a Modified Many-Body Dispersion Correction. *J. Phys. Chem. Lett.* **2016**, *7*, 3278.

(52) Kim, M.; Kim, W. J.; Gould, T.; Lee, E. K.; Lebegue, S.; Kim, H. uMBD: A Materials-Ready Dispersion Correction That Uniformly Treats Metallic, Ionic, and van der Waals Bonding. *J. Am. Chem. Soc.* **2020**, *142*, 2346.

(53) Shishkin, M.; Sato, H. DFT+U in Dudarev′s formulation with corrected interactions between the electrons with opposite spins: The form of Hamiltonian, calculation of forces, and bandgap adjustments. *J. Chem. Phys.* **2019**, *151*, 024102.

Graphical TOC Entry

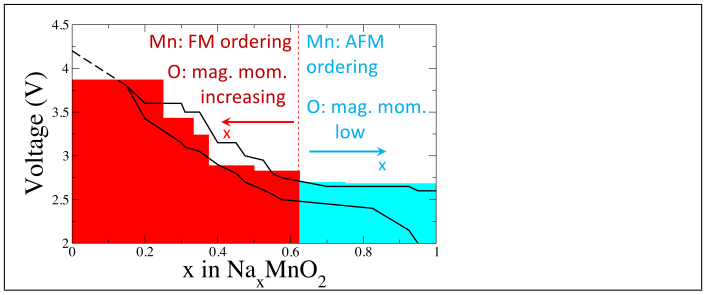

Some journals require a graphical entry for the Table of Contents. This should be laid out "print ready" so that the sizing of the text is correct.
Inside the `tocentry` environment, the font used is Helvetica 8 pt, as required by *Journal of the American Chemical Society*.
The surrounding frame is 9 cm by 3.5 cm, which is the maximum permitted for *Journal of the American Chemical Society* graphical table of content entries. The box will not resize if the content is too big: instead it will overflow the edge of the box.
This box and the associated title will always be printed on a separate page at the end of the document.